Quaternary Geochronology 73 (2022) 101382

Contents lists available at ScienceDirect

Quaternary Geochronology

journal homepage: www.elsevier.com/locate/quageo

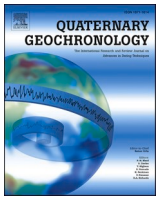

Testing the accuracy of OSL and pIR IRSL dating of young geoarchaeological sediments in coastal Peru

J. Sanjurjo-Sánchez [a,b,*], W. Viveen [a,b], R. Vega-Centeno Sara-Lafosse [b,c]

[a] Grupo Interdisciplinar de Patrimonio Cultural y Geológico, Instituto Universitario de Geología "Isidro Parga Pondal", Universidad de A Coruña, ESCI, Campus de Elviña, 15071, A Coruña, Spain
[b] Grupo de Investigación en Geología Sedimentaria. Especialidad de Ingeniería Geológica, Departamento de Ingeniería, Pontificia Universidad Católica del Perú, San Miguel, Lima, Peru
[c] Sección de Arqueología, Departamento de Humanidades, Pontificia Universidad Católica del Perú, Av. Universitario, 1801, San Miguel, Lima, Peru

ARTICLE INFO

Keywords:
Rimac valley
Human occupation
Fluvial sediments
pIR IRSL dating

ABSTRACT

Luminescence dating of late Quaternary sediments in Peru is challenging, especially on the Peruvian coast. Earlier studies have shown that quartz grains often exhibit a thermally unstable, medium signal that caused the underestimation of Optically Stimulated Luminescence (OSL) ages. InfraRed Stimulated Luminescence (IRSL) dating has shown to produce more reliable ages, depending, amongst other factors, on the age model (Central or Minimum Age Model), and the IRSL signal. IRSL dating of geoarchaeological sediments has, however, hardly been carried out, let along validated, against an independent age dataset. This dating approach is, nonetheless, the only promising way to date the geological substrate in which many of Peru's archaeological sites are buried. Peru contains some of the oldest and most important archaeological heritage sites, yet not much is known of the environmental context in which many of its early civilizations prospered. A better understanding of which luminescence method works best could therefore help in a better understanding of the geological-stratigraphical context of many of Peru's sites.

To investigate this matter more fully, we compared the luminescence dating results of seven sediment samples from the top layer of the Lima alluvial fan and from geoarchaeological layers of the Maranga Complex (San Miguel, Lima), with an independent dataset of sixteen ^{14}C ages. Our results showed that the quartz OSL ages always underestimated the expected ages due to a signal dominated by medium and slow components, and that the post-IR $IRSL_{225}$ ($pIR\ IRSL_{225}$) and $IRSL_{50}$ ages of K-feldspars, on basis of the Central Age Model (CAM), always overestimated the expected ages. The Minimum Age Model (MAM) on the other hand, correctly predicted the expected ages for the early Holocene, Lima alluvial fan sediments using the pIR $IRSL_{225}$ signal of K-feldspars, and the late Holocene, geoarchaeological ages using the $IRSL_{50}$ signal.

1. Introduction

The prehistory of Peru includes the earliest civilizations of America (Shady et al., 2001; Shady, 2006; Mauricio et al., 2021) and some of the most spectacular human structures, including Machu Picchu and the Nazca lines. There are, however, enormous gaps in geoarchaeological knowledge (Sandweiss et al., 2009) despite, but in part because of, the high density of uninvestigated archaeological sites and the highly dynamic nature of geological, geomorphological and climatic processes during the late Quaternary (Lamb and Davis, 2003; Rigsby et al., 2003). And whilst the database of ^{14}C-dated (Rademaker et al., 2013) and luminescence-dated (Roque et al., 2004; Feathers et al., 2008; Vaughn et al., 2014; Mejia-Bernal et al., 2020; Galli et al., 2020; Marsh et al., 2021) archaeological artefacts steadily grows, the geological substrate in which many of the sites are buried, and which provide clues for the context of environmental change during human occupation, remains largely undated. The only cases of luminescence dating of sediments of archaeological sites, that we are aware of, are by Rink and Bartoll (2005), who dated the geoglyphs of the Nazca lines; and Feathers et al. (2019) who dated rocks and sediments in the Peruvian coastal desert.

The application of luminescence dating in Peru is, from a methodological perspective, of particular interest because it was observed that

* Corresponding author. Grupo Interdisciplinar de Patrimonio Cultural y Geológico, Instituto Universitario de Geología "Isidro Parga Pondal", Universidad de A Coruña, ESCI, Campus de Elviña, 15071, A Coruña, Spain.
E-mail address: jorge.sanjurjo.sanchez@udc.es (J. Sanjurjo-Sánchez).

https://doi.org/10.1016/j.quageo.2022.101382
Received 1 December 2021; Received in revised form 22 June 2022; Accepted 26 June 2022
Available online 15 August 2022

the Blue-OSL (BL-OSL) signal of quartz is not always suitable for dating. Steffen et al. (2009) reported a thermally unstable, medium signal that caused the underestimation of the BL-OSL ages in fluvial sediments of the Peruvian coast. But they did get reliable pIR IRSL ages for these sediments. Another study, on the other hand, did report reliable BL-OSL ages when compared to radiocarbon ages of fluvial and lacustrine samples in the Peruvian Andes (Viveen et al., 2019). Dated fluvial sediments in the Amazon region of Peru provided reliable quartz BL-OSL ages for some samples (Viveen et al., 2021), while for others not due to a thermally unstable, medium BL-OSL component. In the latter case, pIR IRSL dating of K-feldspars had to be carried out (Viveen et al., 2020). Baby et al. (2021) successfully dated fluvial cave sands in the Amazon region and speculated that the thermally unstable, medium component of the quartz BL-OSL observed on the coast could be related to the bedrock source of the quartz, which is different along the Peruvian coast when compared to the central and eastern Andes.

In summary, the use of quartz for BL-OSL dating on the Peruvian coast is not recommended and K-feldspar IRSL dating would be the wiser choice. But K-feldspar dating of young, Holocene sediments is also problematic, due to the daylight exposure required for bleaching the IRSL signals, and due to an unbleachable component that ubiquitously exists in fully-bleached samples (Madsen et al., 2011; Buylaert et al., 2012; Murray et al., 2014). Thus, the reliability of K-feldspar IRSL signals for dating late Holocene sediments is still a topic of scientific debate. More information regarding its applicability is, however, needed because it is the only alternative to date the geological substrate surrounding the Peruvian archaeological coastal sites, which are among the earliest and most important prehistoric human occupations in the world (Mauricio et al., 2021).

The aim of this work is therefore to assess the reliability of quartz BL-OSL and K-feldspar pIR IRSL dating of Holocene, geoarchaeological sediments. As a study site, we have chosen the Maranga Complex in Lima, the capital city of Peru, which sits on top of the large, 20-km-wide Lima alluvial fan. The recent publication of sixteen ^{14}C ages of archaeological layers from our research site (Vega-Centeno et al., 2021) enabled us to independently compare our BL-OSL and pIR IRSL ages with these ^{14}C results. This will guide us towards a better understanding of the limitations and strengths of luminescence dating and how future dating of geoarchaeological sediments can be improved.

As a second objective, we will also establish the age of the latest phase of aggradation of the Lima alluvial fan, which is situated directly underneath the archaeological complex of Maranga. Attempts to date the Lima fan so far have resulted in contradicting results. ^{10}Be-dating of the uppermost part of the fan yielded 490 ± 80 ka, whereas the basal part of the fan, some 30 m below the former, was dated at 490 ± 70 ka (Litty et al., 2019). Luminescence ages of the fan using quartz grains, however, returned much younger ages of 44.5 ± 3.1 ka at 8.6 m below the fan surface and 55.3 ± 4.5 ka at 8.5 below the fan surface in Magdalena district (Villacorta et al., 2019), some ~ 4 km south of our study area. However, the use of quartz for BL-OSL dating in this area is not recommended (Steffen et al., 2009) and Villacorta et al. did not report details about the BL-OSL signals, making it difficult to assess the reliability of their ages.

2. Study area

The urban complex of Maranga on the south bank of the Rimac River covers more than 100 ha in what must have been the largest human

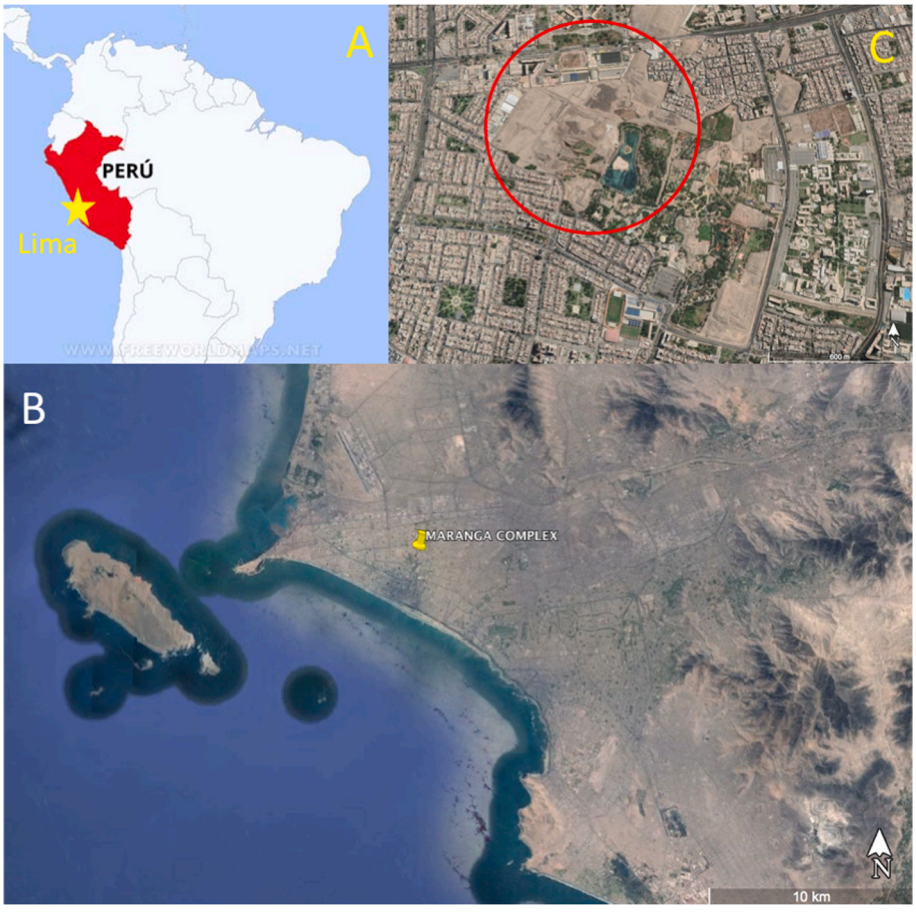

Fig. 1. (A) Map with the location of Peru and its capital city Lima. (B) Google Earth view of the Lima alluvial fan with the location of the Parque de las Leyendas. (C) Situation of the Maranga Complex in the Parque de las Leyendas.

settlement on the central coast of Peru in the first millennium AD. (Fig. 1A). This complex is currently located within the urban area of the city of Lima. An important section of the complex is located within the grounds of the Parque de las Leyendas (the municipal zoo) (see Figs. 1B and 2C). A section, up to 50 m long and up to 6 m deep, was excavated in the 1980s, and has been a topic of study ever since. Various authors have shown that only the upper 2.5 m corresponded to human occupational layers and that the lower part contained natural alluvial fan sediments (Valdez and Jacay, 2012; Vega-Centeno et al., 2021). The most recent study identified fifteen archaeological and natural, alluvial stratigraphic levels (see Fig. 2A, B and 2C) that were ^{14}C-dated by means of sixteen samples (Vega-Centeno et al., 2021). The archaeological layers contained six generations of patio floors and supporting layers with artificial fill that was used as a basis on which the patio floors were laid out (layers O to J and layer E in Fig. 2B). The younger layers I to A (excluding E) are typically grey-yellow gravelly to sandy fluvial layers containing ceramic shards, hinting at episodic inundation of the area. These geoarchaeological layers are easily distinguished from the underlying, natural alluvial fan sediments which are coarse-fabric, clast--supported conglomerates in a reddish, sandy to loamy matrix. The sixteen ^{14}C ages from layers O to E (Fig. 2B) revealed that human occupation took place between 1396 and 1236 years ago (Vega-Centeno et al., 2021), a time span that corresponded to the Lima Culture time. Lima style ceramics recovered from the profile confirmed the ^{14}C results (Vega-Centeno et al., 2021).

3. Methods

3.1. Sampling

Eight samples for luminescence dating were collected by hammering steel tubes in sandy alluvial strata from the Maranga profile. Samples PDL-1 and -2 were located some ~20 m south of the section with occupational levels (see Fig. 2A, B and 2C). They were taken from small sand lenses embedded in the conglomerates of the uppermost, undisturbed part of the Lima alluvial fan. Based on a projected continuation of the oldest occupational level, PDL-1 and PDL-2 are situated 0.9 m beneath this occupational level. Samples PDL-3 and -4 were taken from yellowish-grey, coarse sandy fluvial channel fills containing ceramic shards that, based on their relative elevation in the profile, correlate with the ^{14}C-dated archaeological layers (Fig. 2A, B and 2C). Samples PDL-5 and -6 were taken from a stratigraphic profile directly adjacent to the main profile (Fig. 2A), and can also be correlated to layers I to A as they share the existence of the same fluvial channel fills containing grey,

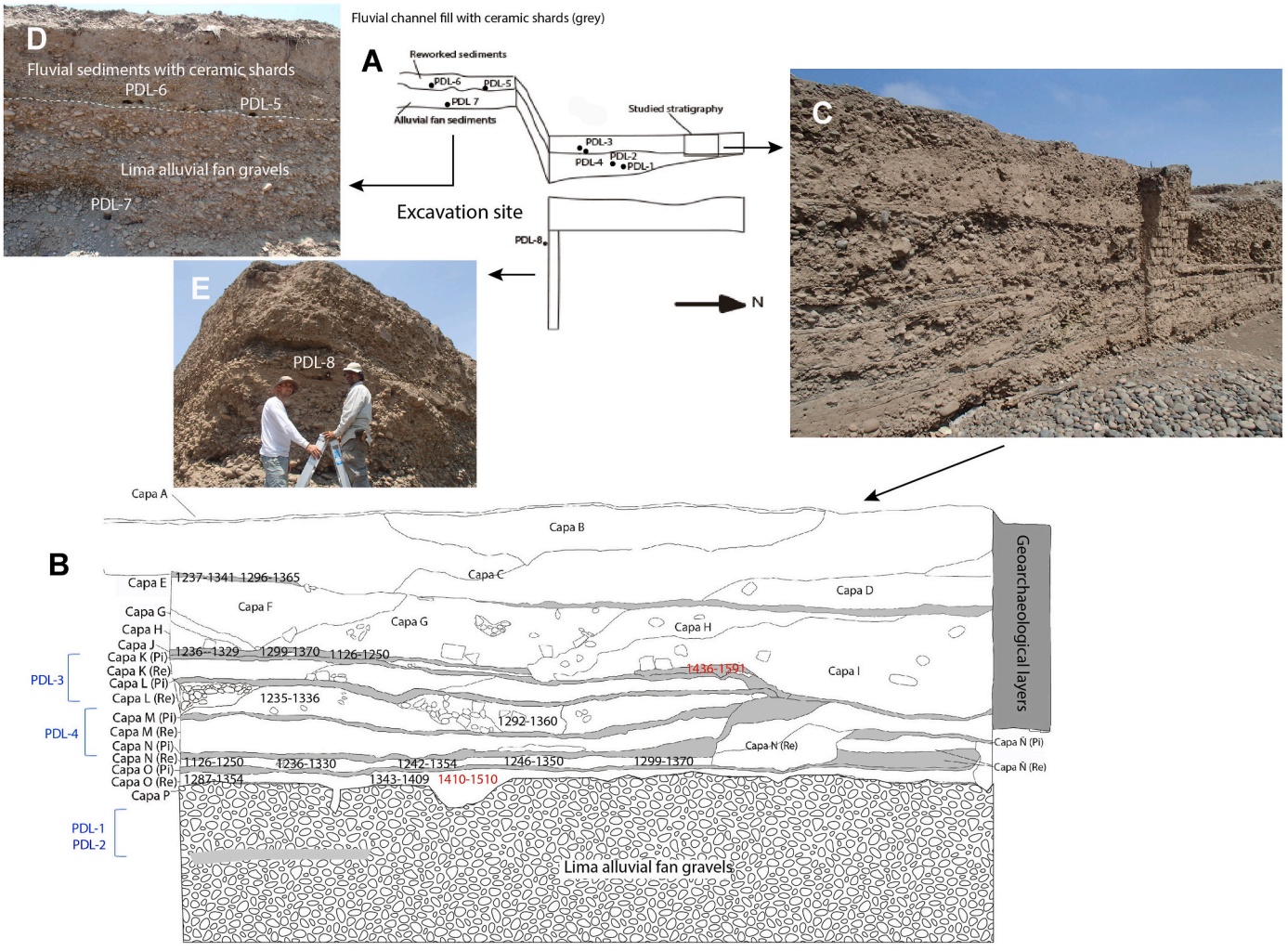

Fig. 2. (A) Overview of the studied stratigraphic section and location of samples PDL-1 to PDL-8. (B) Stratigraphic section from Vega Centeno et al. (2021). ^{14}C ages in years before present, where present is the year of sampling in 2016. Black ages are reliable ages and red ages overestimated the expected ages, as discussed in Vega Centeno et al. (2021). Projected locations of samples PDL-1 to PDL-4 given in blue. (C) Picture of the stratigraphic section shown in (B). (D) Section with locations of samples PDL-5 and PDL-6 in younger, fluvial sediments with ceramic shards; and sample PDL-7 which was taken from the reddish, natural conglomerates of the alluvial fan. (E) Picture of the profile where sample PDL-8 was taken.

medium to coarse sand and reworked materials such as ceramic shards (Fig. 2D). The sediments where samples PDL-5 and -6 were taken overlie the reddish, natural conglomerates from the Lima alluvial fan (Fig. 2D). From a coarse sand layer in between these alluvial fan conglomerates sample PDL-7 was extracted (Fig. 2A and D). Sample PDL-8 was taken from fluvial channel sands containing ceramic shards which also correspond to the occupational layers mentioned above (Fig. 2A and E).

3.2. Equivalent doses

The tubes were opened under red light in the luminescence lab of the University of A Coruña. Grains from the central part of the cores were dried and sieved to get medium-sized grains of 180–250 μm. The grains were treated with hydrochloric acid and hydrogen peroxide to remove carbonates and organic matter. The dried feldspars and heavy minerals were removed by density separation, using sodium polytungstate solutions with densities of 2.62 g cm^{-3} and 2.70 g cm^{-3}. The remaining quartz fraction was etched in concentrated hydrofluoric acid (40%) during 1 h to remove any remaining feldspars. This etching removed approximately 10 μm of the quartz surfaces that received an additional alpha dose during burial. Hydrochloric acid was applied again to remove any remaining soluble fluorides after which the grains were dried. Aliquots of all samples were checked with infrared (IR) stimulation to ensure the absence of contamination by minerals other than quartz. Pure K-feldspar coarse grains were also obtained from the <2.58 g cm^{-3} separate of the central part of the cores and etched with HF to remove the external coating of the grains. They were used for pIR IRSL dating. Neither quartz nor K-feldspar grains were obtained for sample PDL-6. Thus, this sample was dismissed for further dating.

For luminescence measurements, both an automated Risø DA-15 TL/OSL reader system and a Lexsyg Research TL/OSL reader were used. The Risø reader was equipped with blue light-emitting diodes (LEDs), and signals were recorded with a coupled 9235QA photomultiplier tube (PMT). Laboratory doses were given using a $^{90}Sr/^{90}Y$ beta source emitting a 0.100 ± 0.003 Gy s^{-1} dose to samples of the measured geometry. The Lexsyg reader was equipped with a PMT Hamamatsu for recording luminescence signals while the beta source emitted a 0.095 ± 0.003 Gy s^{-1} dose.

Small, multi-grain aliquots of quartz grains were mounted on stainless steel discs and measured by placing optical Hoya U-340 filters (6 mm-thick) in both devices to measure the UV range emission. The blue-OSL (BL-OSL) single-aliquot regenerative dose (SAR) protocol (Murray and Wintle, 2000, 2003) was used to stimulate aliquots for 40 s at 125 °C, using the first 0.4 s to measure BL-OSL and the last 4 s for background subtraction.

K-feldspar grains were measured in both luminescence readers using a combination of Schott-BG 39 and Corning 7–59, and Schott-BG 39 and BrightLine HC414/46 glass filters in the Risø and Lexsyg readers, respectively. A single aliquot regenerative dose (SAR) protocol was used for dating, with a IRSL signal stimulated at 225 °C after a preceding IR stimulation at 50 °C (pIR $IRSL_{225}$) (Thomsen et al., 2008). Before measurements, preheat tests were performed showing negligible changes in the obtained equivalent doses (D_es), with recycling and recuperation ratios at preheat temperatures ranging between 200 and 300 °C for 60 s. A preheat temperature of 300 °C was chosen.

Residual signals were measured for subtraction of the residual dose from the obtained D_es on both signals after daylight bleaching for a week. Dose-recovery tests were performed on bleached aliquots and anomalous fading tests were carried out following Auclair et al. (2003). All IR signals were measured and normalised with a test dose (L_x/T_x) after different storage times between irradiation (with a subsequent preheat) and measurements. The obtained L_x/T_x were plotted against time delay (log scale) between irradiation and measurement to assess the *g-values* (see Figs. S1 and S2). These values were used to calculate fading-corrected ages (Huntley and Lamothe, 2001).

3.3. Dose rates

To assess the dose rates (D_r), the ^{40}K and ^{238}U, ^{235}U and ^{232} Th day chain activities were estimated using Low Background Gamma Spectrometry. The D_rs were assessed using the conversion factors of Guérin et al. (2011). For quartz, the alpha contribution was neglected and the beta dose-rate were corrected (Brennan, 2003) as a result of the HF etching step. For K-feldspar grains, the estimation considered an internal beta dose estimated by assuming a K-content of 12.5 ± 0.5% (Huntley and Baril, 1997). As K-feldspar grains were etched in HF, an external alpha dose was not considered. The water content and saturation state of the samples was assessed in the laboratory and an average water content was estimated based on these values. The cosmic dose rates were calculated according to Prescott and Hutton (1994).

3.4. OSL signal analysis

To study the OSL signals in more detail, we carried out linearly, modulated, optically stimulated luminescence measurements (LM-OSL). This approach was firstly suggested by Bulur (1996) to identify and isolate the individual components that make up the continuous wave (CW) OSL signals from quartz (Bailey et al., 1997; Jain et al., 2003; Kiyak et al., 2007). Deconvolution of the LM-OSL decay curves is usually performed to assess the contribution of each component to the CW-OSL signals (Kitis et al., 2007, 2008, 2011; Polymeris et al., 2008) and more specifically for assessing the D_es. We used quartz multigrain aliquots of samples PDL-2 and PDL-7 for this purpose as they provided some of the brighter OSL signals. Measurements were carried out for natural and regenerated signals. Linearly modulated (LM) blue stimulation for 1000 s at a stimulation temperature of 125 °C was carried out on natural and regenerated signals (15.2 Gy) after a 200 °C preheat for 10 s. This was done on multigrain aliquots in a Risø DA-15 automated reader under the same conditions as the continuous wave (CW) OSL measurements performed for assessing the D_es.

Deconvolution of LM-OSL signals was performed using the spreadsheet of Konstantinidis et al. (2021). They created a built-in function of Lambert W in Excel. The spreadsheet is derived according to the One Trap One Recombination (OTOR) model explained by Chen and Pagonis (2011). The spreadsheet is iterative and the user can insert some random values for the maximum intensity of the LM-OSL peak (I_m), the time that corresponds to that peak (t_m), and the retrapping ratio (R). The spreadsheet allows to run the solver add-in, thereby trying to minimize the Figure Of Merit (FOM value, %). The FOM was proposed by Balian and Eddy (1977) and used to show whether the theoretically obtained curve matches satisfactorily with the experimental one.

4. Results

All samples showed very similar ^{238}U and ^{232}Th activity concentrations, ranging from 28 ± 6 to 33 ± 7 Bq ka^{-1} and from 33 ± 3 to 49 ± 2 Bq ka^{-1}, respectively (see Table 1). Both decay chains did not show any evidences of disequilibrium. The activity concentration of ^{40}K was also similar for all samples, ranging from 551 ± 26 to 690 ± 39 Bq kg^{-1}. They provided estimated D_rs that ranged from 2.61 ± 0.08 to 3.21 ± 0.11Bq kg^{-1} and from 3.55 ± 0.16 to 4.22 ± 0.18 Bq kg^{-1} for medium-sized quartz and K-feldspar grains.

BL-OSL measurements on medium quartz grains showed slow and dim signals for all samples (see Fig. 3A). Despite this, the signals were integrated to obtain equivalent doses (D_e) (see Table 2). As we mentioned in the Introduction, a thermally unstable, medium BL-OSL component has been described in quartz grains from various areas in Peru (Steffen et al., 2009; Viveen et al., 2020). To check if such an unstable component was present in the BL-OSL signals, we built $D_e(t)$ plots for all samples. They showed decreasing $D_e(t)$ (see Fig. 3B), that confirmed that the integration of the OSL signal in the first seconds of the OSL decay curve provided a different result (higher D_es) when

Table 1
Activity concentration of ^{238}U, ^{235}U and ^{232} Th day chains and ^{40}K; and estimated Dose Rates (D_r) for quartz and K-feldspar grains.

Sample	Depth (m)	^{40}K (Bq/kg)	^{238}U (Bq/kg)	^{226}Ra (Bq/kg)	^{232}Th (Bq/kg)	^{235}U (Bq/kg)	Quartz D_r (Gy ka^{-1})	k-feld D_r (Gy ka^{-1})
PDL-1	3.4	626 ± 31	33 ± 6	36 ± 2	39 ± 2	2.1 ± 0.5	3.09 ± 0.08	4.08 ± 0.16
PDL-2	3.3	551 ± 26	30 ± 6	32 ± 4	33 ± 3	0 ± 0	2.61 ± 0.08	3.55 ± 0.16
PDL-3	1.3	583 ± 27	31 ± 6	36 ± 4	43 ± 2	0 ± 0	3.00 ± 0.10	4.00 ± 0.17
PDL-4	1.5	647 ± 37	33 ± 7	36 ± 2	49 ± 2	2.9 ± 0.7	3.18 ± 0.10	4.10 ± 0.17
PDL-5	2.2	651 ± 40	30 ± 6	43 ± 3	42 ± 2	4.2 ± 0.8	3.21 ± 0.11	4.22 ± 0.18
PDL-7	4.5	690 ± 39	30 ± 6	36 ± 2	46 ± 2	2.4 ± 0.6	3.18 ± 0.10	4.15 ± 0.13
PDL-8	2.0	584 ± 28	28 ± 6	31 ± 4	38 ± 2	0 ± 0	2.74 ± 0.09	3.70 ± 0.16

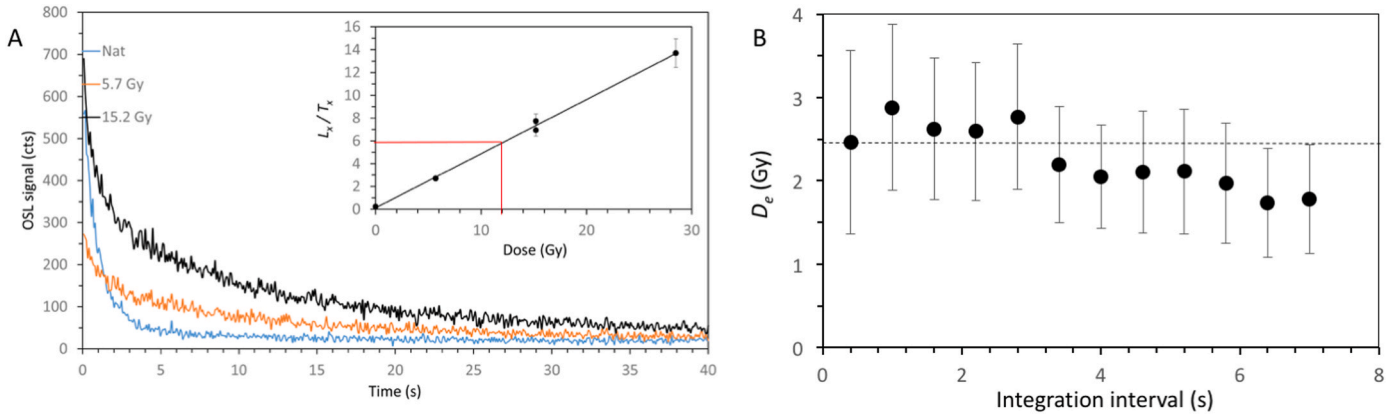

Fig. 3. (A) Decay curves of BL-OSL of quartz multigrain aliquots (sample PDL-1) and dose-response curve (inset); (B) D_e(t) plot of an aliquot of sample PDL-1 that shows a decreasing D_e with increasing integration intervals.

Table 2
Results of BL-OSL dating of quartz multigrain aliquots and resulting ages with the CAM and MAM. N: number of accepted aliquots; D_e (equivalent dose); OD: overdispersion.

Sample	N	De (Gy)		OD (%)	OSL Age (y)	
		CAM	MAM		CAM	MAM
PDL-1	38	10.00 ± 0.79	4.77 ± 0.35	44.4 ± 6.0	3239 ± 270	1544 ± 123
PDL-2	43	9.78 ± 0.85	3.12 ± 0.23	52.9 ± 6.5	3752 ± 347	1199 ± 95
PDL-3	52	3.19 ± 0.26	1,39 ± 0.39	52,3 ± 6.1	1063 ± 92	461 ± 131
PDL-4	52	3.20 ± 0.27	1.83 ± 0.47	52.4 ± 6.6	1007 ± 90	577 ± 149
PDL-5	47	2.25 ± 0.19	1.14 ± 0.04	54.2 ± 6.4	701 ± 64	355 ± 17
PDL-7	50	9.,81 ± 0.51	3.70 ± 0.73	35.0 ± 4.1	3084 ± 189	1163 ± 233
PDL-8	55	1.78 ± 0.15	0.85 ± 0.01	53.8 ± 6.5	648 ± 58	308 ± 11

compared to the use of a broader integration interval. Steffen et al. (2009) also remarked that the relative contributions of both the fast and medium components were different in natural and regenerated signals due to this unstable component. We observed the same behavior in our samples (Fig. 3A).

The deconvolution analyses carried out on natural and regenerated curves of samples PDL-2 (Fig. 4A and B, respectively) and PDL-7 (Fig. 4C and D, respectively) revealed the presence of four components with different contributions to the LM-OSL. The FOM of all signals was high, ranging from 3.7% to 14%. We used a multiplication factor of 1000, although the authors of the spreadsheet remarked that this is not absolutely necessary. We used the factor because it improved the fit and deconvolution of the very dim signals we obtained. What was common to all signals was the low, fast component. A second, medium component was dominant in regenerated signals for sample PDL-2 (~36%), while a third, slow component was dominant in the regenerated signals of sample PDL-7 (~31%). For natural signals, both the third and fourth slow components were observed, while the first, fast component and the second, medium component were negligible. Thus, the lack of a dominant fast signal (Kitis et al., 2011) suggests that the SAR protocol is not reliable for the studied samples.

In addition, we carried out anomalous fading tests on the OSL signals of samples PDL-4 and PDL-7 (see Fig. S3), following the methodology of Auclair et al. (2003). OSL signals were measured and normalised with a test dose (L_x/T_x) on used aliquots (after SAR measurements). OSL measurements were carried out using different storage times between irradiation (using a later preheat) and measurements. The obtained L_x/T_x were plotted vs. time delay (log scale) between irradiation and measurement (Huntley and Lamothe, 2001). Very dim and weak signals were obtained, and negligible fading was observed for the OSL signals (Fig. S3). This showed that the cause of the age underestimation observed from quartz grains was not caused by an anomalous fading in quartz grains, as earlier reported by Fragoulis and Readhead (1991), nor by to feldspar inclusions or by volcanic quartz (Bonde et al., 2001; Tsukamoto et al., 2007). Rather, the underestimation seems to be caused by medium and slow components dominating the OSL signals.

Despite this, and for the sake of comparing the BL-OSL ages with the ^{14}C and pIR IRSL ages, we performed preheat tests on quartz aliquots to choose a suitable preheat temperature. Results (Fig. 5A and B) provided poor recycling and high recuperation ratios. We selected a preheat temperature that minimized recuperation and maximized recycling ratios, which were different for several samples. This was not always easy (see Fig. 5B) as some samples provided high recuperation ratios and poor recycling ratios for all preheat temperatures. As a consequence, a high number of aliquots was rejected after SAR measurements. After the selection of a preheat temperature for all samples (ranging between 220 °C and 260 °C), we used the SAR protocol for multigrain aliquots and selected the aliquots that met the SAR requirements. Based on the aliquots we used, we applied the Central Age (CAM) and Minimum Age Models (MAM) of Galbraith et al. (1999) to assess tentative ages for the

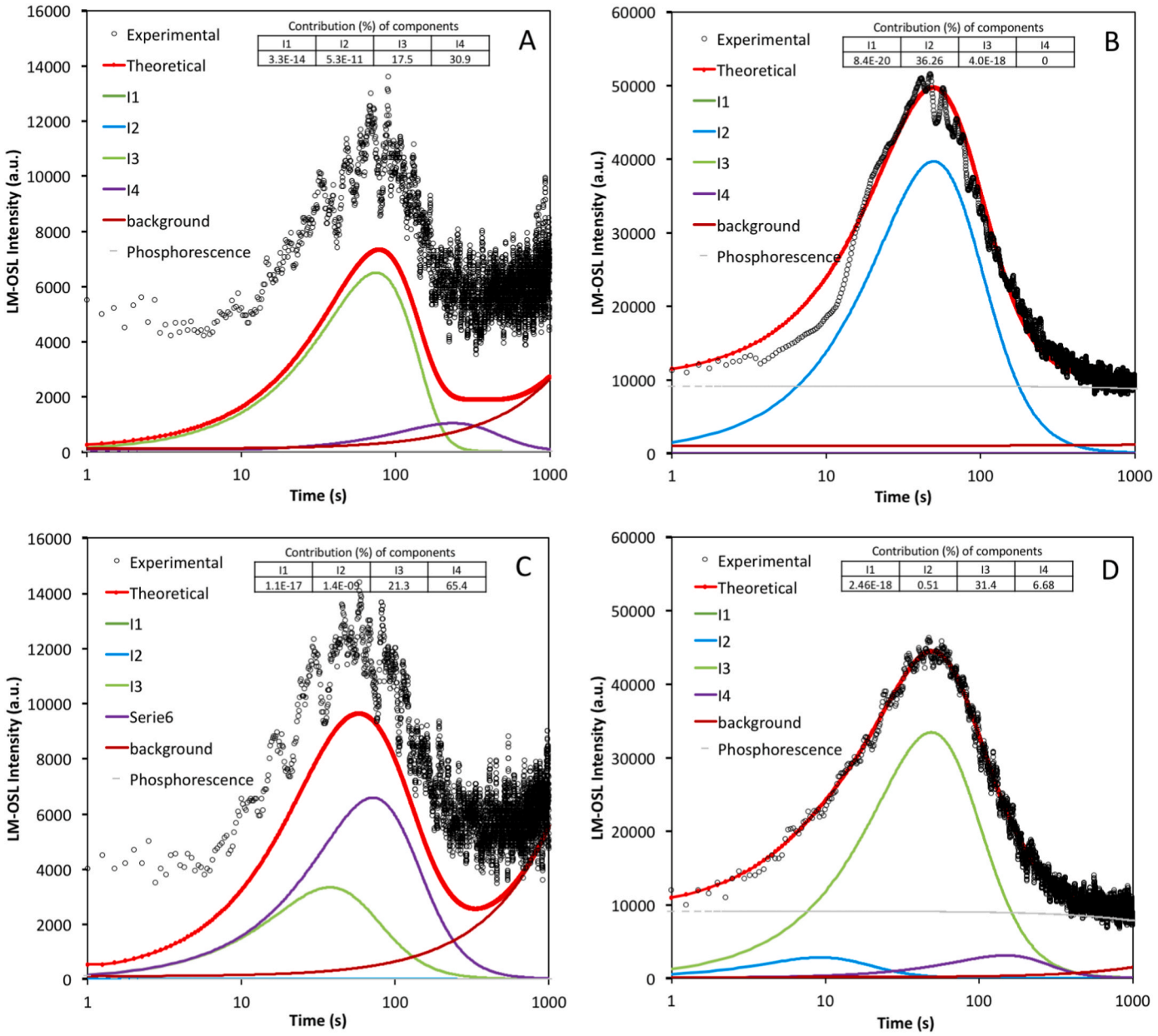

Fig. 4. (A) Deconvolution of the LM-OSL signals for sample PDL-2. (B) Deconvolution of the LM-OSL signals for sample PDL-7. (C and D) Performed with the spreadsheet provided by Kitis et al. (2011). Natural LM-OSL (A and C) shows dim signals dominated by I3 and I4 components, while regenerated signals (after providing a 15.2 Gy beta dose) are dominated by an I2 component. The contribution (%) of each component was estimated and provided in the table inset in each plot.

BL-OSL quartz signal (Table 2).

For K-feldspar dating we did a first IRSL measurement at 50 °C ($IRSL_{50}$) and then one pIR IRSL signal measurement at 225 °C. The latter was chosen because it provided good results in other Peruvian Andean studies (Viveen et al., 2020) and in young sediments (Rhodes, 2015). The $IRSL_{50}$ signals of the K-feldspar grains exhibited bright signals (see Fig. 6A), while pIR $IRSL_{225}$ signals were dim (see Fig. 6B). We performed preheat tests for both signals on all samples. We observed a plateau between 260 °C and 300 °C for all samples and therefore we chose a preheat temperature of 300 °C for 60 s (Fig. 6C and D). We estimated the equivalent doses, and fading tests allowed the correction of the $IRSL_{50}$ ages. For the pIR $IRSL_{225}$ signal, negligible fading was observed (see obtained *g-values* in Table 3 and Fig. S2). The overdispersion values of the central mean for both $IRSL_{50}$ and pIR $IRSL_{225}$ signals ranged from 20% to 50%, suggesting that incomplete bleaching caused the age overestimation. Thus, we used the MAM to assess the age of K-feldspars. Smedley et al. (2019), for instance, suggested that feldspars provide a similar accuracy and precision as quartz does in alluvial sediments. Although the overdispersion values for K-feldspars are high, not all samples showed skewed distributions (see distributions of sample PDL-1 in Fig. 7A and B; and of PDL-4 in Fig. 7C and D). In particular, the D_e distributions of the pIR $IRSL_{225}$ signals were not skewed in most samples, and this signal showed negligible fading, while D_es obtained from the $IRSL_{50}$ signal were more skewed. This is probably due to the use of multigrain aliquots. We then calculated apparent K-feldspar ages based on the CAM and MAM (Table 3).

5. Discussion

Samples PDL-1, PDL-2 and PDL-7 corresponded to the undisturbed

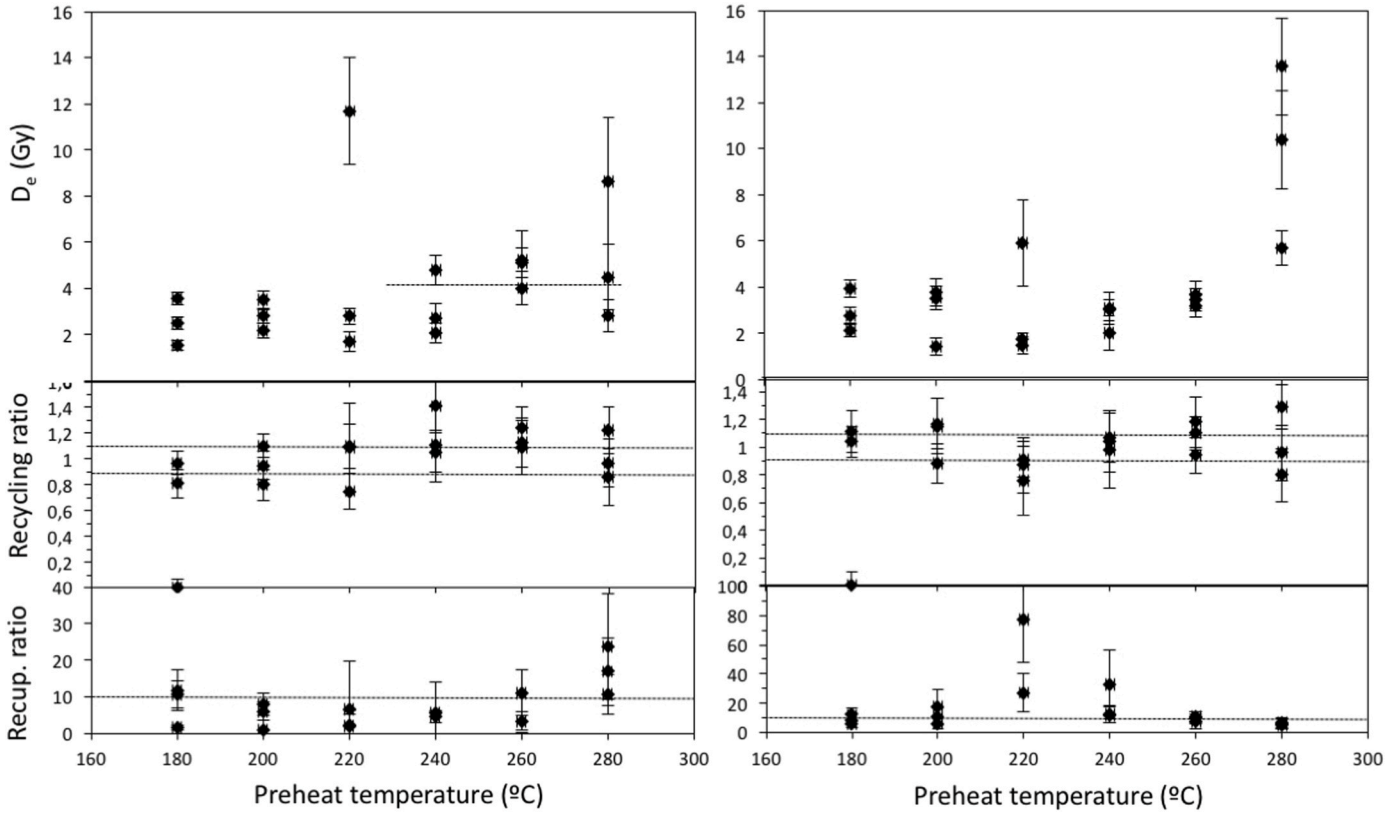

Fig. 5. Preheat tests of quartz OSL signals for samples (A) PDL-5 and (B) PDL-4. For sample PDL-5 a plateau was observed from a 240° to 280 °C preheat temperature, but with poor recycling and high recuperation ratios at these temperatures. For sample PDL-4 no clear plateau was observed. Recycling ratios were poor and recuperation ratios were high for temperatures between 200° and 260 °C.

layers of the Lima alluvial fan. The BL-OSL signal of quartz grains provided ages ranging from 3752 ± 347 y (years before sampling in the year 2017) to 3084 ± 189 y using the CAM and ages from 1544 ± 123 y to 1163 ± 233 y using the MAM (Table 2). These ages are much younger than expected when compared to the ages that were obtained by Villacorta et al. (2019) and Litty et al. (2019), see Introduction. Available ages of alluvial fans and fluvial terraces elsewhere along the Peruvian coast all show major aggradation phases during the late Pleistocene and early Holocene, but never during the late Holocene (Steffen et al., 2009, 2010; Trauerstein et al., 2014; Litty et al., 2018).

The BL-OSL ages from samples PDL-3, PDL-4, PDL-5 and PDL-8 that were extracted from the geoarchaeological layers can be compared against the ^{14}C ages obtained from the adjacent ^{14}C-dated profile (Fig. 2). These ^{14}C ages provided a narrow time interval of 1396 y to 1236 y for the entire occupational history (Vega-Centeno et al., 2021). Our obtained BL-OSL age ranged from 1063 ± 92 y to 648 ± 58 y using the CAM; and from 577 ± 149 y to 308 ± 11 y using the MAM (Table 2). It is therefore clear that the quartz BL-OSL ages underestimated the expected ages. This agrees with the LM-OSL signal deconvolution of two of the studied samples (Fig. 4A–D), which already showed that the behavior of quartz OSL signals is not suitable for the SAR protocol (Wintle and Murray, 2006). This is due to the dominant medium and slow components observed. So, we discard anomalous fading (Fragoulis and Readhead, 1991; Bonde et al., 2001; Tsukamoto et al., 2007) as the possible cause of age underestimation using the SAR OSL on quartz grains. Under these circumstances quartz is not recommended for luminescence dating on the Peruvian coast, as reported here and by Steffen et al. (2009), in contrast to other areas of Peru where quartz can be used to calculate reliable ages (Viveen et al., 2019, 2020; Baby et al., 2021). It would be desirable to study the OSL signals of quartz on the Peruvian coast in more detail for its potential applicability to date archaeological sediments, but this is beyond the scope or this work.

The MAM using the $IRSL_{50}$ and pIR $IRSL_{225}$ signals of K-feldspar grains provided coherent, corrected ages for samples PDL-1, PDL-2 and PDL-7 (Table 3). Five out of six of the calculated ages gave 9.5 ± 3.0 ky to 11.8 ± 0.6 ky and only one, much older, $IRSL_{50}$ age of 17.5 ± 2.4 ky. The CAM on the other hand, returned a much larger spread in the $IRSL_{50}$ and pIR $IRSL_{225}$ ages ranging from 13.9 ± 1.8 ky to 23.0 ± 3.4 ky.

The $IRSL_{50}$ and pIR $IRSL_{225}$ signals of samples PDL-3, PDL-4; PDL-5 and PDL-8 provided corrected CAM ages ranging from 1770 ± 192 y to 15.6 ± 1.6 ky that clearly overestimated the ^{14}C ages (Table 3 and Fig. 2). The same occurred with the MAM ages estimated with the pIR $IRSL_{225}$ signals that ranged from 1762 ± 353 y to 3260 ± 1031 y. MAM ages obtained with the fading-corrected $IRSL_{50}$ signal, however, gave results ranging from 849 ± 250 y to 1580 ± 332 y, which are coherent with the ^{14}C ages. The overestimation of the ages with the pIR $IRSL_{225}$ signal is probably due to an unbleachable component that ubiquitously exists in fully-bleached samples (Buylaert et al., 2012; Murray et al., 2014), and which typically affects young (e.g., late Holocene) samples (Madsen et al., 2011).

Our results very clearly demonstrated that quartz BL-OSL dating results in underestimation of the expected ages, both for early and late Holocene samples. The pIR $IRSL_{225}$ and $IRSL_{50}$ ages do better, but it is paramount to consider carefully which age model and which IRSL signals to use. The CAM resulted in an overestimation of all IRSL ages, whereas the MAM correctly predicted most of the expected IRSL ages. Using the MAM, the pIR $IRSL_{225}$ signal worked better for the natural alluvial fan sediments of early Holocene age, while the $IRSL_{50}$ signal worked better for the late Holocene, geoarchaeological sediments.

Our results clearly showed that the Lima alluvial fan ceased to aggradate at the onset of the Holocene. But it is only around 1750 years ago that there is evidence of large urban centers such as Maranga, Makat Tampu or Pucllana spread out over the southern margin of the valley during the Lima Culture. Current data does not allow a satisfactory

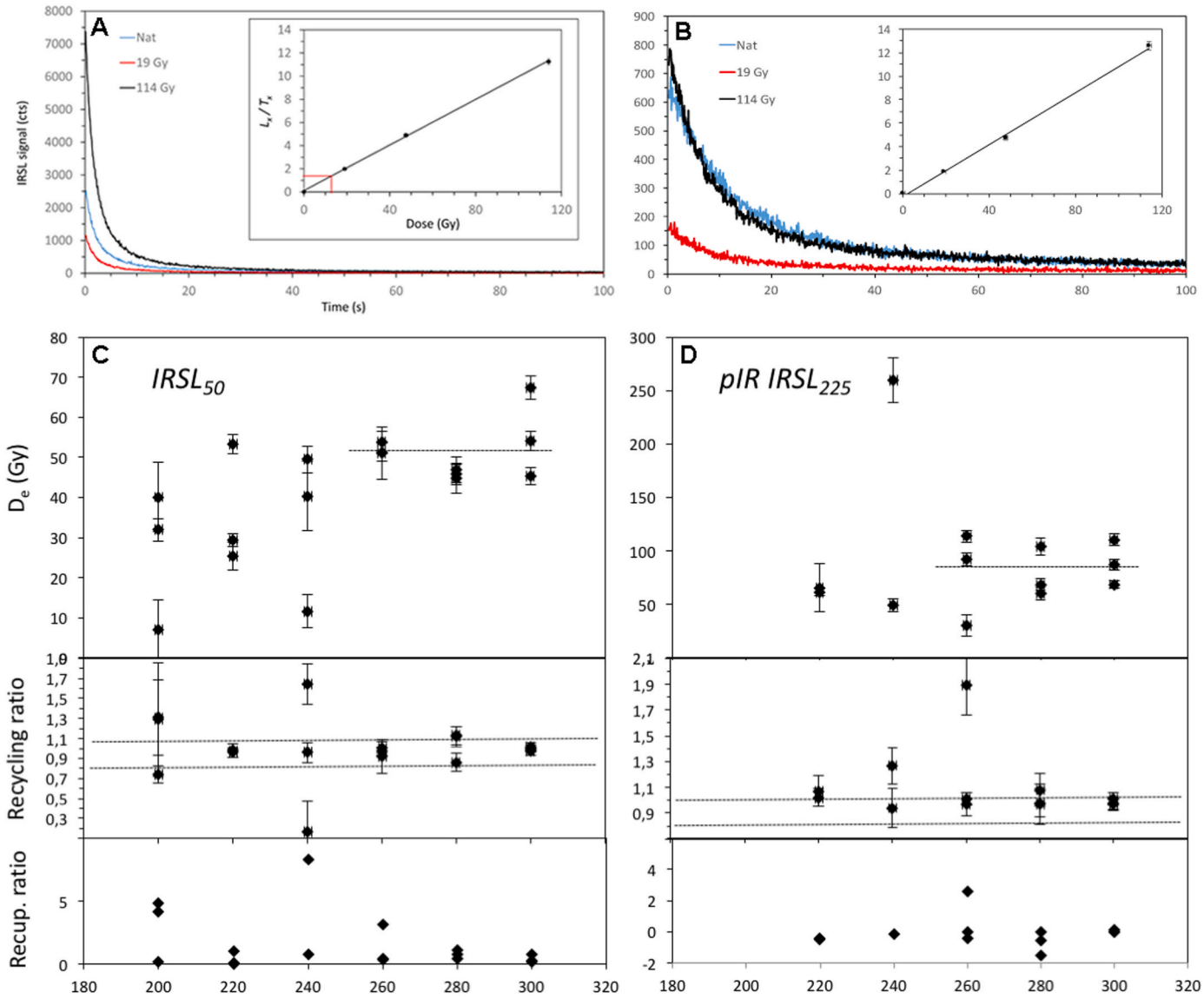

Fig. 6. (A) Example of $IRSL_{50}$ and (B) pIR $IRSL_{225}$ decay curves (with dose-response curves in the insets) of sample PDL-1. Preheat test for (C) $IRSL_{50}$ and (D) pIR $IRSL_{225}$ signals for the same sample. There was a plateau for both signals between 260° and 300 °C preheat temperature, with good recuperation and recycling ratios.

Table 3
Results of IRSL dating of K-feldspar multigrain aliquots with $IRSL_{50}$ and pIR $IRSL_{225}$ signals, and resulting ages with the CAM and MAM. Apparent ages are corrected for $IRSL_{50}$ signals considering the estimated *g-value*. For pIR $IRSL_{225}$, negligible fading was observed, so no fading correction was performed. N: number of accepted aliquots; D_e (equivalent dose).

Sample	Signal	D_e (Gy)			Uncorrected Age			Corrected Age	
		CAM	MAM	N	CAM	MAM	g-value (%)	CAM	MAM
PDL-1	$IRSL_{50}$	47.9 ± 2.1	31.5 ± 1.6	21	11.1 ± 0.7 ky	7.6 ± 0.6 ky	3.48 ± 1.69	14.7 ± 4.1 ky	10.1 ± 2.4 ky
	pIR $IRSL_{225}$	68.9 ± 4.0	50.8 ± 1.3	18			–	16.3 ± 1.2 ky	11.8 ± 0.6 ky
PDL-2	$IRSL_{50}$	50.5 ± 1.6	39.1 ± 2.0	21	13.8 ± 0.8 ky	10.5 ± 0.8 ky	5.18 ± 0.76	23.0 ± 3.4 ky	17.5 ± 2.4 ky
	pIR $IRSL_{225}$	62.9 ± 3.1	40.3 ± 2.9	20			–	17.0 ± 1.2 ky	10.7 ± 1.0 ky
PDL-3	$IRSL_{50}$	9.82 ± 0.60	5.81 ± 0.41	26	2039 ± 184 y	1035 ± 127 y	5.28 ± 1.34	3.18 ± 0.61 ky	1580 ± 332 y
	pIR $IRSL_{225}$	29.4 ± 3.5	16.5 ± 3.0	13			–	6.1 ± 0.3 ky	3260 ± 1031 y
PDL-4	$IRSL_{50}$	20.5 ± 2.1	5.35 ± 0.26	27	4.74 ± 0.55 ky	1038 ± 131 y	1.5 ± 1.1	5.35 ± 0.85 ky	1160 ± 601 y
	pIR $IRSL_{225}$	65.5 ± 6.1	13.3 ± 2.1	23			–	15.6 ± 1.6 ky	2825 ± 560 y
PDL-5	$IRSL_{50}$	8.3 ± 0.3	5.95 ± 0.26	31	1591 ± 117 y	1032 ± 96 y	1.44 ± 0.95	1770 ± 192 y	1150 ± 139 y
	pIR $IRSL_{225}$	15.8 ± 1.3	11.4 ± 0.7	12			–	3.58 ± 0.40 ky	2028 ± 224 y
PDL-7	$IRSL_{50}$	53.8 ± 4.7	30.3 ± 5.6	24	12.6 ± 1.2 ky	7.0 ± 1.4 ky	3.85 ± 1.14	22.3 ± 5.3 ky	9.7 ± 2.5 ky
	pIR $IRSL_{225}$	62.6 ± 10.9	44.3 ± 12.4	13			–	13.9 ± 1.8 ky	9.5 ± 3.0 ky
PDL-8	$IRSL_{50}$	7.6 ± 0.5	3.63 ± 0.52	23	1801 ± 174 y	728 ± 166 y	2.8 ± 1.7	2240 ± 449 y	849 ± 250 y
	pIR $IRSL_{225}$	14.7 ± 2.0	8.4 ± 3.8	12			–	2860 ± 510 y	1762 ± 353 y

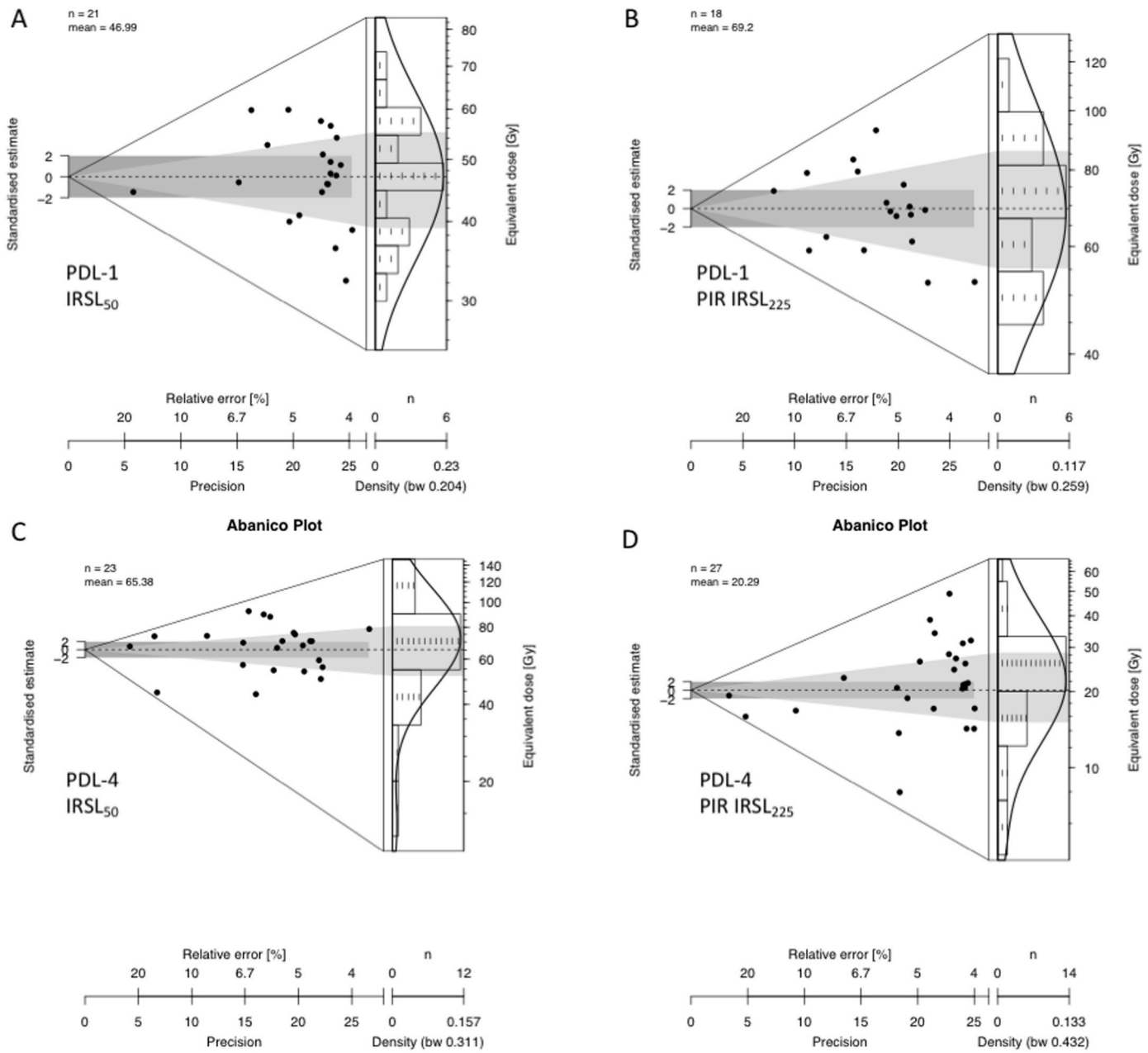

Fig. 7. (A) Abanico plot (D_e) of the $IRSL_{50}$ signal and (B) pIR $IRSL_{225}$ signal for sample PDL-1. (C) Abanico plot (D_e) of $IRSL_{50}$ signal and (D) pIR $IRSL_{225}$ signal for sample PDL-4. The grey shaded areas correspond to the central age (CAM).

explanation for the reason of this late occupation of the southern Rimac margin. Vega-Centeno et al. (2021) suggested that the preceding occupation of the northern margin might be related to the better conditions for agriculture, as it is an area in close proximity to the Chillón River. This confluence might have generated a more suitable land for simple agricultural practices, whereas the southern margin required large scale irrigation facilities in order to become agriculturally productive.

6. Conclusions

BL-OSL and IRSL dating of Holocene, natural and archaeological sediments of the Peruvian coast allowed a better evaluation of which dating method works best there. A comparison with a published record of ^{14}C ages shows that quartz BL-OSL ages always underestimated the expected ages. Indeed, the deconvolution of the natural and regenerated LM-OSL signals of two of the studied samples showed that the signal was dominated by medium and slow components. This is the most probable cause of age underestimation and not anomalous fading as previously reported.

For k-feldspars, the CAM, on basis of pIR $IRSL_{225}$ and $IRSL_{50}$ signals, always overestimated the expected ages. The MAM provided the expected ages, but the pIR $IRSL_{225}$ signal worked better for early Holocene, natural sediments, whereas the $IRSL_{50}$ signal worked better for late Holocene, geoarchaeological sediments. Our results showed that aggradation of the Lima fan halted at the onset of the Holocene, contrary to proposals of other workers.

Declaration of competing interest

The authors declare that they have no known competing financial interests or personal relationships that could have appeared to influence the work reported in this paper.

Acknowledgements

The research for this paper benefitted from two grants of the Palarq Foundation (Spain) for our research project "Estudio interacción hombre-ambiente en los procesos de población del valle del Rímac en Lima, Perú". Partial funding was provided by the Program "Consolidación y estructuración de unidades de investigación competitivas: Grupos de potencial de crecimiento" (ED431B 2021/17) of the Xunta de Galicia. The Management of the Parque de las Leyendas (San Miguel, Lima) is kindly acknowledged for the permissions that allowed us to study and sample the site. We also would like to thank the editor and an anonymous reviewer for valuable comments that improved the quality of this paper. Funding for open access charge: Universidade da Coruña/CISUG.

Appendix A. Supplementary data

Supplementary data to this article can be found online at https://doi.org/10.1016/j.quageo.2022.101382.

References

Auclair, L.J., Lamothe, M., Huot, S., 2003. Measurement of anomalous fading for feldspar IRSL using SAR. Radiat. Meas. 37, 487–492.
Baby, P., Viveen, W., Sanjurjo-Sánchez, J., Bigot, J.-Y., Dosseto, A., Villegas-Lanza, J.C., Apaéstegui, J., Guyot, J.-L., 2021. First record of OSL-dated fluvial sands in a tropical Andean cave reveals rapid late Quaternary tectonic uplift. Terra. Nova 33, 262–273.
Balian, H.G., Eddy, N.W., 1977. Figure-of-merit (FOM), an improved criterion over the normalized chi-squared test for assessing goodness-of-fit of gamma-ray spectral peaks. Nucl. Instrum. Methods 145, 389–395.
Bailey, R.M., Smith, B.W., Rhodes, E.J., 1997. Partial bleaching and the decay form characteristics of quartz OSL. Radiat. Meas. 27, 123–136.
Bonde, A., Murray, A., Friedrich, W.L., 2001. Santorini: luminescence dating of a volcanic province using quartz? Quat. Sci. Rev. 20, 789–793.
Brennan, B.J., 2003. Beta doses to spherical grains. Radiat. Meas. 3, 299–303.
Bulur, E., 1996. An alternative technique for optically stimulated luminescence (OSL) experiment. Radiat. Meas. 26, 701–709.
Buylaert, J.P., Jain, M., Murray, A.S., Thomsen, K.J., Thiel, C., Sohbati, R., 2012. A robust feldspar luminescence dating method for Middle and Late Pleistocene sediments. Boreas 41, 435–451.
Chen, Reuven, Pagonis, Vasilis, 2011. Thermally and Optically Stimulated Luminescence: A Simulation Approach. Willey.
Feathers, J.K., Johnson, J., Kembel, S.R., 2008. Luminescence dating of monumental stone architecture at chavín de huántar, perú. J. Archaeol. Method Theor 15, 266–296.
Feathers, J., More, G.M., Quinterosc, P.S., Burkholder, J.E., 2019. IRSL dating of rocks and sediments from desert geoglyphs in coastal Peru. Quat. Geochronol. 49, 177–183.
Fragoulis, D.V., Readhead, M.L., 1991. Feldspar inclusions and the anomalous fading and enhancement of thermoluminescence in quartz grains. Int. J. Radiat. Appl. Instrum. Nucl. Tracks Radiat. Meas. 18, 291–296.
Galbraith, R.F., Roberts, R.G., Laslett, G.M., Yoshida, H., Olley, J.M., 1999. Optical dating of single and multiple grains of quartz form Jinmi-um Rock Shelter, northern Australia: Part I, experimental design and statistical models. Archaeometry 41, 339–364.
Galli, A., Panzeri, L., Rondini, P., Pogggiani Keller, R., Martini, M., 2020. Luminescence.
Guérin, G., Mercier, N., Adamiec, G., 2011. Dose-rate conversion factors: update. Ancient TL 29, 5–8.
Huntley, D.J., Baril, M.R., 1997. The K content of the K-feldspars being measured in optical dating or in thermoluminescence dating. Ancient TL 15, 11–13.
Huntley, D.J., Lamothe, M., 2001. Ubiquity of anomalous fading in K-feldspars and the measurement and correction for it optical dating. Can. J. Earth Sci. 38, 1093–1106.
Jain, M., Murray, A.S., Bøtter-Jensen, L., 2003. Characterisation of blue light stimulated luminescence components in different quartz samples: implications for dose measurement. Radiat. Meas. 37, 441–449.
Kiyak, N.G., Polymeris, G.S., Kitis, G., 2007. Component resolved OSL dose response and sensitization of various sedimentary quartz samples. Radiat. Meas. 42, 144–155.
Kitis, G., Pagonis, V., 2008. Computerized curve deconvolution analysis for LM-OSL. Radiat. Meas. 43, 737–741.
Kitis, G., Polymeris, G.S., Kiyak, N.G., 2007. Component resolved thermal stability and recuperation study of the LM–OSL curves of four sedimentary quartz samples. Radiat. Meas. 42, 1273–1279.
Kitis, G., Polymeris, G.S., Kiyak, N.G., Pagonis, V., 2011. Preliminary results towards the equivalence of transformed continuous-wave optically stimulated luminescence (CW-OSL) and linearly-modulated (LM-OSL) signals in quartz. Geochronometria 38, 209–216.
Konstantinidis, P., Kioumourtzoglou, S., Polymeris, G.S., Kitis, G., 2021. Stimulated luminescence; Analysis of complex signals and fitting of dose response curves using analytical expressions based on the Lambert W function implemented in a commercial spreadsheet. Appl. Radiat. Isot. 176, 109870.
Lamb, S., Davis, P., 2003. Cenozoic climate change as a possible cause for the rise of the Andes. Nature 425, 792–797.
Litty, C., Schlunegger, F., Akçar, N., Delunel, R., Christl, M., Vockenhuber, C., 2018. Chronology of alluvial terrace sediment accumulation and incision in the Pativilca Valley, western Peruvian Andes. Geomorphology 315, 45–56.
Litty, C., Schlunegger, F., Akçar, N., Lanari, P., Christl, M., Vockenhuber, C., 2019. Possible climatic controls on the accumulation of Peru's most prominent alluvial fan: the Lima Conglomerate. Earth Surf. Process. Landforms 44, 991–1003.
Madsen, A.T., Buylaert, J.P., Murray, A.S., 2011. Luminescence dating of young coastal deposits from New Zealand using feldspar. Geochronometria 38, 379–390.
Mauricio, A.C., Grieseler, R., Heller, A.R., Kelley, A.R., Rumiche, F., Sandweiss, D.H., Viveen, W., 2021. The earliest adobe monumental architecture in the Americas. Proc. Natl. Acad. Sci. USA 118, 1–11.
Marsh, E.J., Korpisaari, A., Mundt, S.P., Gasco, A., Durán, V., 2021. Radiocarbon vs. luminescence dating of archaeological ceramics in the Southern Andes: a review of paired dates, bayesian models, and a pilot study. Radiocarbon 63, 1471–1501.
Mejia-Bernal, J.-R., Ayala-Arenas, J.S., Cano, N.F., Rios-Orihuela, J.F., Gonzales-Lorenzo, C.D., Watanabe, S., 2020. Dating and determination of firing temperature of ancient potteries from Yumina archaeological site, Arequipa, Peru. Appl. Radiat. Isot. 155, 108930.
Murray, A.S., Wintle, A.G., 2000. Luminescence dating of quartz using an improved single-aliquot regenerative-dose protocol. Radiat. Meas. 32, 57–73.
Murray, A.S., Wintle, A.G., 2003. The single aliquot regenerative dose protocol: potential for improvements in reliability. Radiat. Meas. 37, 377–381.
Murray, A.S., Schmidt, E.D., Stevens, T., Buylaert, J.P., Markovic, S.B., Tsukamoto, S., Frechen, M., 2014. Dating Middle Pleistocene loess from Stari Slankamen (Vojvodina, Serbia) - limitations imposed by the saturation behaviour of an elevated temperature IRSL signal. Catena 117, 34–42.
Polymeris, G.S., Kiyak, N.G., Kitis, G., 2008. Component resolved bleaching study of the blue LM-OSL signal of various quartz samples. Geochronometria 32, 79–85.
Prescott, J.R., Hutton, J.T., 1994. Cosmic ray contributions to dose rates for luminescence and ESR dating: large depths and long term variations. Radiat. Meas. 23, 497–500.
Rademaker, K., Bromley, G.M.R., Sandweiss, D.H., 2013. Peru archaeological radiocarbon database, 13,000e7000 14C B.P. Quat. Int. 301, 34–45.
Rhodes, E.J., 2015. Dating sediments using potassium feldspar single-grain IRSL: initial methodological considerations. Quat. Int. 362, 14–22.
Rigsby, C.A., Baker, P.A., Aldenderfer, M.S., 2003. Fluvial history of the Rio Illave Valley, Peru, and its relationship to climate and human history. Palaeogography, Palaeoclimatology, Palaeoecology 194, 165–185.
Rink, W.J., Bartoll, J., 2005. Dating the geometric Nasca lines in the Peruvian desert. Antiquity 79, 390–401.
Roque, C., Guibert, P., Vartanian, E., Vieillevigne, E., Bechtel, F., 2004. Changes in luminescence properties induced by thermal treatments; a case study at Sipan and Trujillo Moche sites (Peru). Radiat. Meas. 38, 119–126.
Sandweiss, D.H., Solís, R.S., Moseley, M.E., Keefer, D.K., Ortloff, C.R., 2009. Environmental change and economic development in coastal Peru between 5,800 and 3,600 years ago. Proc. Natl. Acad. Sci. USA 106, 1359–1363.
Shady, R.S., 2006. In: Isbell, W., Silverman, H. (Eds.), Andean Arqueology III, North and South. Springer Academic Publishing, New York, USA, p. 537.
Shady, R., Haas, J., Creamer, W., 2001. Dating caral, a preceramic site in the supe valley on the central coast of Peru. Science 292 (5517), 723–7226.
Smedley, R.K., Buylaert, J.-P., Újvári, G., 2019. Comparing the accuracy and precision of luminescence ages for partially-bleached sediments using single grains of K-feldspar and quartz. Quat. Geochronol. 53, 101007.
Steffen, D., Schlunegger, F., Preusser, F., 2009. Drainage basin response to climate change in the Pisco Valley, Peru. Geology 37, 491–494.
Steffen, D., Schlunegger, F., Preusser, F., 2010. Late Pleistocene fans and terraces in the Majes valley, southern Peru, and their relation to climatic variations. Int. J. Earth Sci. 99, 1975–1989.
Thomsen, K.J., Murray, A.S., Jain, M., Botter-Jensen, L., 2008. Laboratory fading rates of various luminescence signals from feldspar-rich sediment extracts. Radiat. Meas. 43, 1474–1486.
Trauerstein, M., Lowick, S.E., Preusser, F., Schlunegger, F., 2014. Small aliquot and single grain IRSL and post-IR IRSL dating of fluvial and alluvial sediments from the Pativilca valley, Peru. Quat. Geochronol. 22, 163–174.
Tsukamoto, S., Murray, A.S., Huot, S., Watanuki, T., Denby, P.M., Bøtter-Jensen, L., 2007. Luminescence property of volcanic quartz and the use of red isothermal TL for dating tephras. Radiat. Meas. 42, 190–197.
Valdez, R., Jacay, J., 2012. Cronología, indicadores paleoclimáticos, aluviones y fenómenos de El Niño en la costa central del Perú. Arqueológicas 29, 71–86.
Vega-Centeno, R., Toledo, C., Huamán, L., Alexandrino, G., 2021. Examen de un perfil estratigráfico Lima en Maranga. Late American Antiquity (available on line).
Vaughn, K.J., Eerkens, J.W., CLipo, C., Sakai, S., Schreiber, K., 2014. It's about time? Testing the Dawson ceramic seriation using luminescence dating, Southern Nasca Regio, Peru. Lat. Am. Antiq. 25, 449–461.
Villacorta, S.P., Evans, K.G., Torres, T.J.D., Llorente, M., Prendes, N., 2019. Geomorphological evolution of the Rimac River's alluvial fan, Lima, Peru. Geosci. J. 23, 409–424.
Viveen, W., Zevallos-Valdivia, L., Sanjurjo-Sanchez, J., 2019. The influence of centennial-scale variations in the South American summer monsoon and base-level fall on Holocene fluvial systems in the Peruvian Andes. Global Planet. Change 176, 1–22.

Viveen, W., Sanjurjo-Sanchez, J., Baby, P., González-Moradas, M.d.A., 2021. An assessment of competing factors for fluvial incision: an example of the late Quaternary exorheic Moyobamba basin. Peruvian Subandes. Global and Planetary Change 200, 1–24, 103476.

Viveen, W., Baby, P., Sanjurjo-Sanchez, J., Hurtado-Enríquez, C., 2020. Fluvial terraces as quantitative markers of late Quaternary detachment folding and creeping thrust faulting in the Peruvian Huallaga basin. Geomorphology 367, 1–23.

Wintle, A.G., Murray, A.S., 2006. A review of quartz optically stimulated luminescence characteristics and their relevance in single-aliquot regeneration dating protocols. Radiat. Meas. 41, 369–391.